

and are consistent with prevailing theories for the origin of comets in the outer regions of the sun's pre-planetary accretion disk.

REFERENCES AND NOTES

- V. Vanysek, in *Comets in the Post-Halley Era*, R. L. Newburn et al., Eds. (Kluwer, Dordrecht, Netherlands, 1991), pp. 879–895.
- E. K. Jessberger and J. Kissel, in (7), pp. 1075–1092.
- P. Eberhardt, M. Reber, D. Krankowsky, R. Hodges, *Astron. Astrophys.* **302**, 301 (1995).
- A. Stawikowski and J. Greenstein, *Astrophys. J.* **140**, 1280 (1964).
- A. Danks, D. Lambert, C. Arpigny, *ibid.* **194**, 745 (1974).
- V. Vanysek, in *Comets, Asteroids and Meteorites*, A. H. Delsemme, Ed. (Univ. of Toledo Press, Toledo, OH, 1977), p. 499.
- H. E. Matthews and D. C. Jewitt, *IAU Circular 6567* (1997).
- Most of the observations were carried out in daytime. The JCMT dish is protected from direct solar heating and from wind buffeting by a GoreTex membrane that is transparent to submillimeter wavelengths. Mechanical stability of the JCMT allows pointing to about ± 1.5 arc sec root mean square over much of the sky.
- D. Bockelee-Morvan et al., *Astron. Astrophys.* **141**, 411 (1984).
- D. Bockelee-Morvan, R. Padman, J. K. Davies, J. Crovisier, *Planet. Space Sci.* **42**, 655 (1994).
- Y. X. Cao, Q. Zeng, S. Deguchi, O. Kameya, N. Kaifu, *Astron. J.* **105**, 1027 (1993).
- F. Schloerb, M. J. Claussen, L. Tacconi-Garman, *Astron. Astrophys.* **187**, 469 (1987).
- D. Lis et al., *IAU Circular 6566* (1997).
- E. Anders and N. Grevesse, *Geochim. Cosmochim. Acta* **53**, 197 (1989).
- S. Wyckoff et al., *Astrophys. J.* **339**, 488. (1989).
- M. Kleine, S. Wyckoff, P. Wehinger, B. A. Peterson, *ibid.* **439**, 1021 (1995).
- T. L. Wilson and R. J. Rood, *Annu. Rev. Astron. Astrophys.* **32**, 191 (1994).
- G. Dahmen, T. Wilson, F. Matteucci, *Astron. Astrophys.* **295**, 194 (1995).
- D. Krankowsky et al., *Nature* **321**, 326. (1986).
- Y.-N. Chin, C. Henkel, J. B. Whiteoak, N. Langer, E. B. Churchwell, *Astron. Astrophys.* **305**, 960 (1996).
- M. Frerking, R. W. Wilson, R. A. Luuke, P. G. Wannier, *Astrophys. J.* **240**, 65. (1980).
- We thank the operators of JCMT for their assistance, and B. Marsden and D. Tholen for help with the ephemerides. Supported by a grant from NASA Planetary Astronomy Program to D.C.J.

7 May 1997; accepted 12 August 1997

Midwinter Start to Antarctic Ozone Depletion: Evidence from Observations and Models

H. K. Roscoe,* A. E. Jones, A. M. Lee

Measurements of total ozone at Faraday, Antarctica (65°S), by a visible spectrometer show a winter maximum. This new observation is consistent with the descent of air within the polar vortex during early winter, together with ozone depletion starting in midwinter. Chemical depletion at these latitudes in midwinter is suggested by existing satellite observations of enhanced chlorine monoxide and reduced ozone above 100 hectapascals and by reduced ozone in sonde profiles. New three-dimensional model calculations for 1994 confirm that chemical ozone depletion started in June at the sunlit vortex edge and became substantial by late July. This would not have been observed by most previous techniques, which either could not operate in winter or were closer to the Pole.

Dramatic ozone depletion was first reported at a high-latitude Antarctic site (76°S), where it was observed to start in late August (1). This is the time in the spring when the stratosphere becomes sunlit at this latitude, whereby the photochemistry leading to ozone depletion is initiated. Most subsequent investigations of the ozone hole also concentrated on sites at these high latitudes. There were few investigations at sites further north, because dynamical activity near the edge of the Antarctic vortex made it more difficult to see the depletion. Hence, the ozone hole has usually been

considered to occur exclusively during the spring and often is perceived to be associated with the time of year rather than with the availability of sunlight at that location. The possibility that depletion might occur during winter within the vortex equatorward of 67°S, where there is always enough sunlight to initiate photochemistry, had not been subjected to a conclusive test.

Observations of total ozone during the Antarctic winter are sparse. Reliable observations by a Dobson spectrophotometer cannot be made poleward of 60°S in midwinter (2) because the Dobson observes ultraviolet (UV) light. The satellite-borne Total Ozone Mapping Spectrometer (TOMS) cannot make accurate observations in June or July at 65°S (3) because it also observes solar UV. The satellite-borne Tiros Operational Vertical Sounder (TOVS) has poor accuracy over the central Antarctic plateau in winter and reduced accuracy at the edge of Antarctica

(4). The satellite-borne Microwave Limb Sounder (MLS) can only measure the column of ozone above 100 hPa, only measures south of 40°S for alternate 36-day periods, and was not launched until 1991 (5).

Ozone absorbs visible light, as well as the UV light observed by the Dobson. Observations by a visible spectrometer of light scattered from the zenith sky can be made to 91° solar zenith angle (SZA), that is, throughout the winter at 65°S. In 1990, a ground-based visible spectrometer of the design *Système d'Analyse par Observations Zénithales* [SAOZ (6)] was installed at Faraday (65.3°S, 65.3°W). SAOZ records spectra throughout the day, deducing ozone from absorption between 500 and 560 nm at SZAs between 87° and 91°.

The ability to discern trends in ozone on any time scale is determined by the stability of the measurement calibration. In previous work (7), we examined the stability of measurements of ozone by SAOZ at Faraday and have now improved it (8). The stability of the zero of the measurement is now equivalent to an annual cycle of less than 25 Dobson units (DU) and to a change during winter of less than 10 DU. Hence the measurements by SAOZ at Faraday are the first reliable operational measurements of total ozone throughout the winter at the sunlit edge of the vortex. Although a SAOZ was installed at Dumont d'Urville in 1988 (6), at 140°E the vortex is more often displaced away from that site's side of Antarctica.

We analyzed daily total ozone values in winter for the years 1990, 1991, and 1994 (Fig. 1). Values from 1992 and 1993 were excluded, because air-mass factors (AMFs) of visible light are particularly sensitive to the profile of aerosol in the stratosphere when amounts are large, and the eruption of Mount Pinatubo greatly enhanced aerosol amount and variability in Antarctica for the 2 years from November 1991. This variability makes it difficult to calculate reliable AMFs until 1994, when the amount of aerosol was smaller and less variable (9). A winter maximum in ozone is discernible in all three winters (Fig. 1), especially in the more heavily smoothed lower curves, where the size of the maximum within the winter period is much larger than 10 DU in 1990 and 1991.

The question follows, what is the cause of the observed maximum? There are various mechanisms that might cause an increase in ozone: (i) a decrease in tropopause height, associated with short time-scale synoptic weather systems (10); (ii) the vortex edge moving from one side of Faraday to the other, which certainly results in increased total ozone in the spring over the course of several days, as shown in the large short time-scale fluctuation in Fig. 2 at the end of

H. K. Roscoe and A. E. Jones, British Antarctic Survey, Natural Environment Research Council, High Cross, Madingley Road, Cambridge CB3 0ET, UK.
A. M. Lee, Centre for Atmospheric Science, Department of Chemistry, University of Cambridge, Lensfield Road, Cambridge, CB2 1EW UK.

*To whom correspondence should be addressed at h.roscoe@bas.ac.uk

the 1994 record; (iii) slow descent, which is accompanied by convergence of air aloft with a large mixing ratio of ozone, and possible divergence of air at lower altitudes with a small mixing ratio of ozone. Mechanisms (i) and (ii) give rise to the short time-scale variations in the upper curves of Fig. 1 and are removed by smoothing in the lower curves. Hence they cannot account

for the progressive increase in total ozone observed in May and early June in the SAOZ data. Continuous descent (mechanism iii) in the Antarctic winter stratosphere is now well-established both in models (11–14) and in measurements: Small mixing ratios of N_2O and CH_4 , characteristic of air from higher altitudes, were observed in the Antarctic in spring 1994 (15),

and continuous decline in the column of N_2O above 15 km was observed throughout winter 1994 at the South Pole (16).

Many models predict that descent continues throughout the winter, perhaps slowing down after midwinter (13). None predict ascent after midwinter; and given that the 1994 measurements of N_2O at the South Pole show a continued decline after midwinter (15), there can be no ascent that might cause the decrease in ozone observed in July (Fig. 1). However, there is clearly enough sunlight at 65°S to initiate photochemistry in midwinter, given that SAOZ observes sunlight. Enhanced ClO in the lower stratosphere, formed after heterogeneous conversion of reservoir chlorine ($ClONO_2$ and HCl), was observed at 65°S by MLS in mid-June in 1992 (5) and between late May and mid-June from 1993 to 1997 (17). Ozone-sonde profiles measured at 78°S in June 1994, in air that had moved from 70°S to 50°S before returning, exhibited very large reductions in the amounts of ozone at some altitudes in the lower stratosphere (18), interpreted by the authors as ozone depletion by reactive chlorine.

These measurements of enhanced ClO and of ozone reductions similar to those observed in the spring, together with the availability of sunlight, suggest that the decrease in total ozone observed at Faraday in July arises from chemical destruction.

Two other sets of measurements support a decline in ozone at similar latitudes after midwinter. (i) At Syowa (69.0°S) in 1982, there was an obvious decrease in ozone from lunar Dobson measurements between early July and early August (19). The average of lunar Dobson data from Syowa for the years 1982 to 1994 also shows a decrease by mid-August (20), though it appears smaller than the decrease we observed at Faraday. This is to be expected, because the amount of chlorine available for ozone depletion was less in the 1980s than it is now and because there is less sunlight in midwinter at the latitude of Syowa.

(ii) Decreases in ozone in winter at latitudes near 65°S throughout Antarctica are seen in MLS data. The ozone column above 100 hPa, averaged over the latitude range 60°S to 80°S, showed a continuous decrease from the end of June 1992 and showed a peak at the end of June 1993 (21). Measurements of the ozone mixing ratio at a potential temperature of 465 K show a ring of reduced ozone around the latitude circle of 65°S by 17 August 1992 (22). However, during periods of descent, these observations alone cannot confirm chemical loss. Although convergence occurs aloft, at middle altitudes downward movement of air merely moves the profile downward. Because substantial parts of the ozone column lie below the minimum altitude

Fig. 1. Daily total ozone measured by SAOZ at Faraday at 65°S, using calculated AMFs specific to each month. The upper curves are smoothed by a 5-day running mean for clarity; the lower curves are the same data smoothed by a 41-day running mean. The short time-scale variability in the upper curves, which is even greater in unsmoothed data, agrees with Dobson measurements when available; it is dynamical variability, not noise in the measurements. A winter maximum is discernible in the upper curves, despite this variability, and is more discernible in the lower curves. AMJJAS: April, May, June, July, August, September.

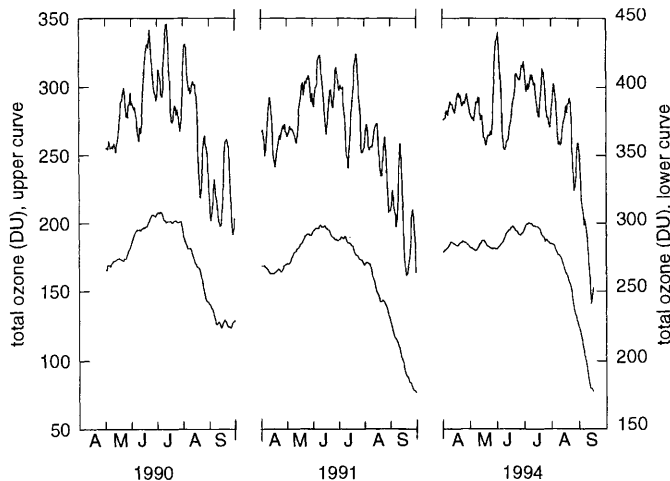
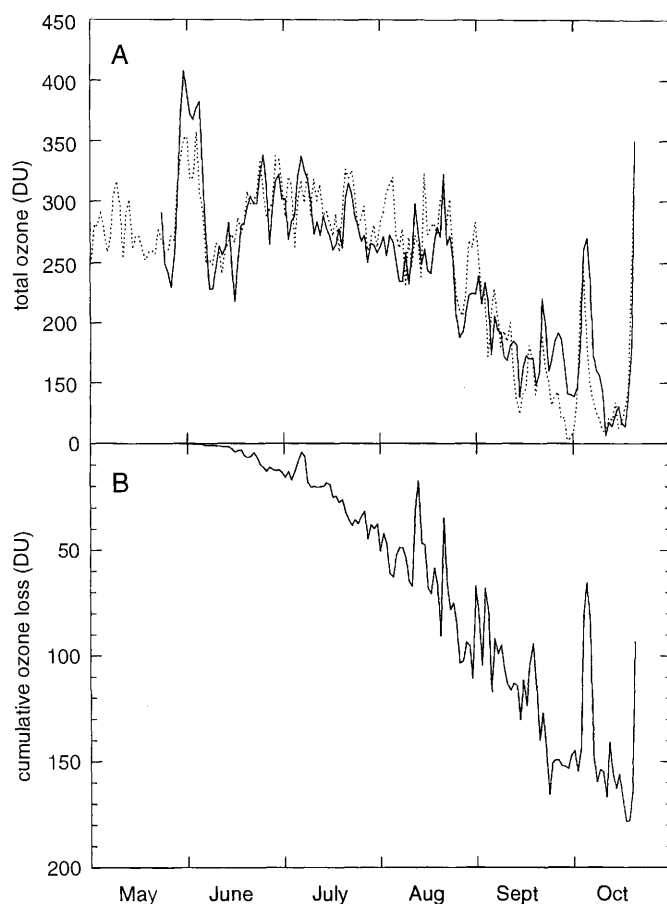


Fig. 2. (A) Daily total ozone measured by SAOZ at Faraday in 1994 (dashed line), compared to total ozone above potential temperature 350 K, calculated by a 3D chemical-transport model (solid line). Neither measured nor calculated ozone values have been smoothed. The model reproduces the large ozone depletion starting in mid-August and reproduces many of the short time-scale dynamical features of the measurements. (B) Accumulated loss in total ozone above 350 K at Faraday in 1994, calculated by the model from cycles involving the formation of the ClO dimer plus the two pathways of ClO + BrO that lead to ozone loss. By mid-August, the calculated depletion frequently exceeds 60 DU.



of MLS observations (100 hPa), during periods of descent progressively more of the ozone column becomes inaccessible to MLS. Descent could cause the decrease in the column above 100 hPa observed by MLS (17) if the accompanying convergence were at a high enough altitude. Manney *et al.* (23) treated this problem by calculations with a dynamical model, which concluded that the change in the vortex-averaged ozone mixing ratio due to descent alone at a potential temperature of 585 K should be an increase of 0.25 parts per million by volume (6%) in the 10 days after 24 June 1992, which is in excellent agreement with the MLS measurements and partially masks a chemical depletion.

Our suggestion that the decrease in total ozone observed at Faraday in July arises from chemical destruction was tested by calculations with the three-dimensional (3D) chemical transport model SLIMCAT (24). This model is formulated in an isentropic vertical coordinate—model levels are surfaces of constant potential temperature. It is an off-line model, whereby temperatures and horizontal winds are specified either from meteorological analyses (as in this study) or from a general circulation model. The vertical motion is derived from the diabatic heating rates calculated with the middle atmosphere radiation code (MIDRAD) of Shine (25). A tracer advection scheme (26) is coupled to a stratospheric chemistry scheme (27), which includes a comprehensive set of gas-phase reactions as well as a detailed treatment of heterogeneous reactions on sulfate aerosol and on polar stratospheric clouds.

For the results presented here, the model was integrated from 24 May 1994 to 21 October 1994 with the use of the 24-hourly analyses of the U.K. Met Office (UKMO) data assimilation system (28). The model had 11 levels, from 350 to 2100 K, and a horizontal resolution of 2.5° latitude by 5.6° longitude. The model was initialized by assimilating profiles of ozone and N₂O data from the upper-atmosphere research satellite (UARS) and profiles of other gases from 2D model results, integrated with the use of potential vorticity and equivalent latitude coordinates (29). The model could not be run in this way for the winters of 1990 or 1991 because UARS data and UKMO analyses do not exist for those years.

The accuracy of the model calculations is confirmed by the good agreement between the calculated and the measured total ozone (Fig. 2A). In particular, the model reproduces many of the short time-scale changes in the measurements, which result from dynamical events, confirming the accuracy of the analyzed winds in this difficult location with large gradients in wind; it reproduces the large ozone depletion (1) in September, confirming the accuracy of the chemical scheme; and it reproduces the smaller decline in ozone during July. Because the lower boundary to the model domain is determined by the 350 K isentropic surface, tracer column amounts are partial column amounts. In particular, model ozone column amounts do not take into account any tropospheric contribution or any stratospheric contribution below the lower boundary. Despite this, the longer time-scale

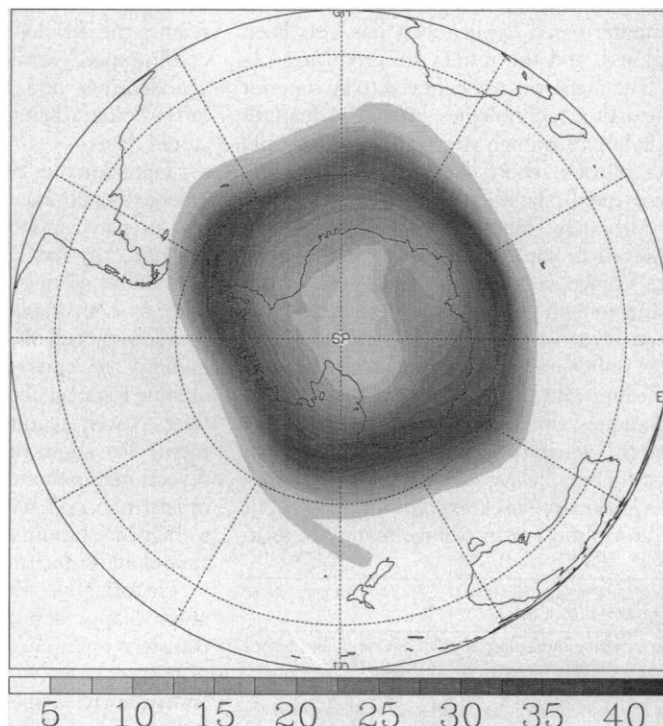
changes over the whole model run are in good agreement with the measurements.

A diagnosis of the model run details the chemical cycles responsible for ozone loss. Over 90% of the ozone loss within the vortex due to reactive halogen compounds arises from the cycles involving the formation of the ClO dimer, and the two pathways of ClO + BrO that lead to ozone loss (Fig. 2B). These model results provide very strong evidence that the observed decrease in ozone from midwinter at Faraday is the result of chemical depletion. Ozone depletion starts in June and reaches significant values (25 DU) by mid-July; by mid-August, the calculated loss reaches 60 DU (Fig. 2B). In the model, the ozone hole develops as a continuous feature at Faraday; there is no sudden start to the ozone loss as observed at Halley in late August (1). It could thus be argued that the ozone hole starts to form in midwinter.

The accumulated ozone loss due to the above cycles near the end of July for the whole of the Southern Hemisphere (Fig. 3) shows that the depletion covers much of a ring at the vortex edge around Antarctica; it is not specific to the location of Faraday. The coherence of the calculated ozone loss in late July (Fig. 3) suggests that mixing between the edge of the vortex and the center is very weak, because otherwise air significantly depleted in ozone would be transported to the Pole by this time. However, this very weak mixing seems to partially contradict some trajectory calculations (30, 31).

We can now substantiate a different concept of the Antarctic ozone hole: In some areas it begins to form in midwinter, not in the spring. The observed winter maxima strongly suggest that depletion regularly starts in midwinter at Faraday. The model shows that the observations are symptomatic of widespread depletion at the sunlit edge of the vortex.

Fig. 3. Accumulated loss in total ozone calculated by the model from cycles involving the formation of the ClO dimer plus both the pathways of ClO + BrO that lead to ozone loss, as in Fig. 2B, but for the whole Southern Hemisphere on 23 July 1994. Significant ozone loss is confined to a ring at the sunlit edge of the vortex, occupying about 5° of latitude centered between 59°S and 72°S and exceeding 35 DU for over half of the ring's circumference. This confinement, more than a month after the start of ozone depletion, illustrates that mixing within the vortex is weak. The gray scale shows the accumulated ozone loss in Dobson units.



REFERENCES AND NOTES

1. J. C. Farman, B. G. Gardiner, J. D. Shanklin, *Nature* **315**, 207 (1985).
2. Direct-sun measurements of total ozone by a Dobson spectrophotometer can only be made at SZA less than 75°, because of the extra extinction of UV from the sun by molecular scattering when the sun is low in the sky. Lunar Dobson observations demand great skill and persistence by the observer, and given their larger scatter than that of normal Dobson measurements (20), they are not considered reliable for medium time-scale trend determination within a single year.
3. TOMS can only make accurate observations, particularly in the presence of polar stratospheric clouds [O. Torres, Z. Ahmad, J. R. Herman, *J. Geophys. Res.* **97**, 13015 (1992)], to about 85° SZA [J.-P. Pommereau *et al.*, in *Proceedings of the 28th Liege International Astrophysics Colloquium*, Liege, Belgium, 26 to 30 June, 1989, P. J. Crutzen, J.-C. Gerard, R. Zander, Eds. (Univ. of Liege, Belgium, 1989), pp. 141–146].
4. TOVS observes upwelling thermal emission from the atmosphere, but its ozone channel relies on a temperature contrast between the surface and the

ozone layer [A. C. Neuendorffer, *J. Geophys. Res.* **101**, 18807 (1996)], and hence in winter it has poor accuracy over the central Antarctic plateau and reduced accuracy at the edge of Antarctica.

5. J. W. Waters *et al.*, *Geophys. Res. Lett.* **20**, 1219 (1993).
6. J.-P. Pommereau and F. Goutail, *ibid.* **15**, 895 (1988).
7. A. E. Jones *et al.*, *J. Quant. Spectrosc. Radiat. Transfer* **54**, 481 (1995).
8. We compared SAOZ ozone to measurements from the Dobson at Faraday in seasons other than winter to test overall stability, and we examined intercepts of Langley plots during all seasons and over a wide range of ozone amounts to test stability of offset. SAOZ observes ozone in the slant path of sunlight through the atmosphere, related to total vertical amount by an air-mass factor (AMF). When observing the zenith sky, sunlight follows a set of parallel paths before being scattered vertically into the instrument, so there is no unique AMF, merely an average AMF that depends on profiles of ozone and air density. By means of a standard radiative transfer scheme [A. Sarkissian, H. K. Roscoe, D. J. Fish, *ibid.*, p. 471], AMFs have now been calculated for each month of the observations, with the use of a mixture of climatological and measured parameters as input.
9. A. Herber *et al.*, *J. Geophys. Res.* **101**, 3921 (1996).
10. G. M. B. Dobson, D. N. Harrison, J. Lawrence, *Proc. R. Soc. London Ser. A* **122**, 456 (1929).
11. M. R. Schoeberl, M. Luo, J. E. Rosenfield, *J. Geophys. Res.* **100**, 5159 (1995).
12. J. D. Mahlman, J. P. Pinto, L. J. Umscheid, *J. Atmos. Sci.* **51**, 489 (1994).
13. J. E. Rosenfield, P. A. Newman, M. R. Schoeberl, *J. Geophys. Res.* **99**, 16677 (1994).
14. G. L. Manney, R. W. Zurek, A. O'Neill, R. Swinbank, *J. Atmos. Sci.* **51**, 2973 (1994).
15. M. C. Abrams *et al.*, *Geophys. Res. Lett.* **23**, 2341 (1996).
16. S. Crewell *et al.*, *J. Geophys. Res.* **100**, 20839 (1995).
17. J. W. Waters, personal communication.
18. H. Vomel, D. J. Hofmann, S. J. Oltmans, J. M. Harris, *Geophys. Res. Lett.* **22**, 2381 (1995).
19. S. Chubachi, in *Proceedings of the Quadrennial Ozone Symposium*, Halkidiki, Greece, 3 to 7 September 1984, C. S. Zerefos and A. Ghazi, Eds. (Reidel, Dordrecht, Netherlands, 1985), pp. 285–289.
20. S. Chubachi, *J. Geophys. Res.* **102**, 1349 (1997).
21. F. Froidevaux *et al.*, *J. Atmos. Sci.* **51**, 2846 (1994).
22. M. L. Santee *et al.*, *Science* **267**, 849 (1995).
23. G. L. Manney *et al.*, *J. Atmos. Sci.* **52**, 3069 (1995).
24. M. P. Chipperfield *et al.*, *J. Geophys. Res.* **101**, 18861 (1996).
25. K. P. Shine, *Q. J. R. Meteorol. Soc.* **113**, 603 (1987).
26. The upstream advection scheme is based on conservation of second-order moments of tracer distribution during advection [M. J. Prather, *J. Geophys. Res.* **91**, 6671 (1986)]. The advection algorithm is stable, accurate, and highly nondiffusive, making the scheme particularly suited to the preservation of sharp gradients, an important consideration where localized chemical processing on polar stratospheric clouds can cause strong inhomogeneities in tracer distributions.
27. M. P. Chipperfield, D. Carriolle, P. Simon, R. Ramaroson, D. J. Lary, *J. Geophys. Res.* **98**, 7199 (1993).
28. R. Swinbank and A. O'Neill, *Mon. Weather Rev.* **122**, 686 (1994).
29. In this study, the model was initialized by assimilating profiles of ozone taken from the MLS data (version 3) [F. Froidevaux *et al.*, *J. Geophys. Res.* **101**, 10,017 (1996)] and profiles of N₂O taken from the cryogenic limb array etalon spectrometer (CLAES) data (version 7) [A. E. Roche *et al.*, *ibid.*, p. 9679]. The MLS and CLAES instruments are on board the upper-atmosphere research satellite (UARS). UARS follows a precessing, 57° inclined orbit. Both MLS and CLAES view in the limb orthogonal to one side of the satellite. In order to view both hemispheres, UARS performs a yaw maneuver every 36 days, so that MLS and CLAES view along the alternate limb. To assemble a near-global set, data from a diurnal cycle

either side of a yaw maneuver was chosen. For this study, MLS ozone from the yaw maneuver that started viewing south on 24 May 1994 was used. Because CLAES ceased to function in 1993, N₂O values from June 1992 were used. Assimilation of these data sets involved binning the data according to their equivalent latitude and potential temperature. Other UARS data could not be used because of internal inconsistency (24), so to complete the initial data set, 2D model values were used. The vertical structure of the model was modified until the model N₂O field was identical to the assimilated N₂O field. The full set of chemical fields from the model was then mapped into the 3D domain with the use of equivalent latitude and potential temperature as the transfer coordinates. These coordinates allow chemical fields to follow polar-vortex distortions in a realistic way.

30. K. P. Bowman, *J. Geophys. Res.* **98**, 23013 (1993).
31. A. M. Lee, H. K. Roscoe, M. P. Chipperfield, R. L. deZafra, D. J. Hofmann, in preparation.
32. We thank J. C. Farman for suggesting that a SAOZ be placed at Faraday; D. J. Oldham for persistence during its first year there; C. J. Wright, S. Cuthbertson, D. Haigh, F. P. Hindle, M. P. Chipperfield, J. A. Pyle, and G. L. Manney for efforts at Faraday in subsequent years; J. Squires for help with Langley plots; A. Sarkissian for AMF software; M. P. Chipperfield and J. A. Pyle for SLIMCAT software; G. L. Manney for discussions on MLS data; and J.-P. Pommereau for first drawing our attention to the hint of a midwinter maximum in ozone from the SAOZ at Dumont d'Urville.

10 June 1997; accepted 11 August 1997

Time-Domain Holographic Digital Memory

Xiao A. Shen, An-Dien Nguyen, John W. Perry,*
David L. Huestis, Ravinder Kachru†

An optical storage technique based on time-domain holography for the rapid recording and readout of page-formatted digital data is demonstrated. Storage of 356 kilobits of data was achieved at a single spatial location in a rare-earth-doped crystal. The digital data were recorded and accurately retrieved at a peak rate of 300 megabits per second without the use of error-correcting codes. The system's raw bit error rate is about 10⁻⁷. This low bit error rate was achieved by a detection scheme for extraction of binary data. These results have implications for dynamic optical memory.

Holographic memories, once considered a storage device of the distant future, have come much closer to reality. Instruments that make use of holographic approaches to data storage have been developed and tested for applications such as the identification of fingerprints (1). Use of spatial holography to store page-formatted digital optical data in computer-based applications has also been explored, and the results are promising (2–4). The memories are believed to be superior to existing technologies, with key features including ultrahigh storage density, rapid data transfer, short data access times, and exceptional reliability.

Although much progress has been achieved in some key areas of holographic data storage, several major technical impediments remain, restricting its application in a broad area, as was promised initially. The most noticeable obstacle has been the slow recording rate of conventional holographic techniques, which record spatial interference patterns generated by two temporally co-existing laser beams. The recording requires, in addition to laser excitation, subsequent electron diffusion in storage materials, as in

the case of photorefractive memory, for example. Such processes limit photorefractive technology to applications that are not input intensive, such as memory that is written only once. Success in developing high-performance input-output (I/O)-intensive holographic memories, such as page-oriented dynamic optical random access memory, will require the development of much higher recording speeds while maintaining high storage densities and low bit error rates, the latter being a benchmark for the quality of stored data.

Time-domain holographic memory has emerged as an excellent candidate for such I/O intensive applications (5, 6). This memory not only has features common to conventional spatial holographic recording, such as high capacity and high degree of parallelism, but also some that are complementary to conventional holography, including fast page recording speed and modest laser power requirement. Recent experiments (6) show that an exposure time of several microseconds and a peak laser power of less than 200 mW are sufficient to record a high-resolution binary image with the time-domain technique.

Historically, the time-domain holographic approach evolved from an optical transient phenomenon known as stimulated photon echoes (7). It is a time-domain or, equivalently, a spectral-domain version of holographic recording. Like conventional

Molecular Physics Laboratory, SRI International, Menlo Park, CA 94025, USA.

*Permanent address: Department of Computer Science and Mathematics, Carleton College, Northfield, MN 55057, USA.

†To whom correspondence should be addressed. E-mail: kachru@mplvax.sri.com